


Elevated Angiotensin-II Levels Contribute to the Pathogenesis of Open-Angle Glaucoma Via Inducing the Expression of Fibrosis-Related Genes in Trabecular Meshwork Cells Through a ROS/NOX4/SMAD3 Axis

Cell Transplantation
Volume 32: 1–18
© The Author(s) 2023
Article reuse guidelines:
sagepub.com/journals-permissions
DOI: 10.1177/09636897231162526
journals.sagepub.com/home/cll


Haijun Li¹, Huiling Cui¹, Jing Ren¹, Di Wang¹, Rumeng Zhao¹, Shichao Zhu², Siqing Liu³, Xiaohui Liu¹, Shuai Tian⁴, Yuanyuan Zhang⁴, Panpan Zhao⁴, Peng Li⁵ , Rick F. Thorne⁴, and Shichao Duan¹ 

Abstract

Glaucoma including primary open-angle glaucoma (POAG) results from elevations in intraocular pressure (IOP). An eye-localized renin-angiotensin system (RAS) has been implicated in IOP regulation, although its mechanism of action and contribution to glaucoma is poorly understood. Here, we detected significant increases in the levels of angiotensin II (ANGII) in aqueous humor samples from POAG patients. Moreover, we determined that the concentrations of ANGII were positively correlated with IOP, suggesting a role for elevated ANGII levels in eye pathogenesis. Functional investigations demonstrated that ANGII induces the expression of fibrosis-related genes of transformed and primary human trabecular meshwork cells (HTMCs) through the transcriptional upregulation of key fibrotic genes. Parallel experiments using a murine periocular conjunctival fornix injection model confirmed that ANGII induces the expression of fibrosis-related genes in trabecular meshwork (TM) cells *in vivo* along with increasing IOP. ANGII was revealed to function through increasing the levels of reactive oxygen species (ROS) via selectively upregulating NOX4, with NOX4 knockdown or inhibition with GLX351322 alleviating fibrotic changes induced by ANGII. We further show that ANGII activates Smad3, with both GLX351322 and an inhibitor of Smad3 (SIS3) decreasing the phosphorylation of Smad3 and dampening the ANGII-induced increases in fibrotic proteins. Moreover, NOX4 and Smad3 inhibitors also partially rescued the elevated IOP levels induced by ANGII. Our collective results therefore highlight ANGII as a biomarker and treatment target in POAG together with establishing a causal relationship between ANGII and up-regulation of the expression of fibrosis-related genes of TM cells via a NOX4/ROS axis in cooperation with TGF β /Smad3 signaling.

Keywords

ANGII, aqueous humor, fibrosis, ROS, NOX4, Smad3, trabecular meshwork

¹ Henan Provincial People's Hospital, Henan Eye Hospital, Henan Eye Institute, Zhengzhou University People's Hospital, Henan University People's Hospital, Zhengzhou, China

² Department of Pharmacology, College of Pharmacy, Army Medical University, Chongqing, China

³ The Second Hospital of Tianjin Medical University, Tianjin Medical University, Tianjin, China

⁴ Translational Research Institute, Henan Provincial People's Hospital, Academy of Medical Science, Zhengzhou University, Zhengzhou, China

⁵ Department of Cardiology, Shanghai Institute of Cardiovascular Diseases, Zhongshan Hospital, Fudan University, Shanghai, China

Submitted: December 8, 2022. Revised: February 18, 2023. Accepted: February 22, 2023.

Corresponding Authors:

Shichao Duan, Henan Provincial People's Hospital, Henan Eye Hospital, Henan Eye Institute, Zhengzhou University People's Hospital, Henan University People's Hospital, Zhengzhou 450003, China.
Email: duanshichao@sibcb.ac.cn

Rick F. Thorne, Translational Research Institute, Henan Provincial People's Hospital, Academy of Medical Science, Zhengzhou University, Zhengzhou 450003, China.
Email: rick.thorne@newcastle.edu.au

Peng Li, Department of Cardiology, Shanghai Institute of Cardiovascular Diseases, Zhongshan Hospital, Fudan University, Shanghai, 200032, China.
Email: lipeng4754@163.com



Introduction

Glaucoma is the principal cause of irreversible blindness, and primary open-angle glaucoma (POAG) is the most common type of glaucoma^{1,2}. Currently, nearly 60.5 million people worldwide are affected by this indolent disorder, with projected estimates this will climb to 111.8 million by the year 2040³. Elevated intraocular pressure (IOP) is the direct cause of glaucoma, with aqueous humor flow is responsible for generating IOP and maintaining normal eye shape. The aqueous humor is produced by the ciliary body and mainly flows out through the trabecular meshwork; hence, abnormalities such as increases in aqueous humor output and/or obstacles to flow serve to promote elevations in IOP⁴.

The solutes of aqueous humor consist of proteins, peptides, hormones, metabolites, and other small molecules. Notably, the aqueous humor is relatively separated from circulation because of the blood-eye barrier, and many factors are generated locally in the eye that function to provide nutrition for intraocular cells. The circulating aqueous humor nourishes the cornea and lens and removes the metabolic waste moving through the ocular chambers and drains from the eye to the venous blood. Nevertheless, altered concentrations or other changes in these constituent molecules can promote various eye diseases including glaucoma, pathologic myopia, cataract, diabetic retinopathy, and age-related macular degeneration⁵⁻¹⁰.

Of relevance to this report is the renin-angiotensin-aldosterone system (RAAS) which plays an essential role in controlling sodium balance and body fluid volumes, and thus serving to regulate blood pressure¹¹. Angiotensinogen (AGT) is cleaved by renin to form angiotensin I, which in turn is processed by angiotensin-converting enzyme (ACE) to angiotensin II, which then activates either the AT1R or the AT2R on the plasma membrane. In addition to the circulatory system that regulates urgent cardiovascular responses, tissue-localized RAS have been shown to influence long-term changes in certain organs¹². For instance, elevated levels of angiotensin II (ANGII) induces skeletal muscle atrophy along with fibrosis in lung, liver, and kidney tissues¹³⁻¹⁶ together with promoting reactive oxygen species (ROS)-mediated stress, senescence, and inflammation¹⁷⁻²⁰. Intriguing, RAS components appear to be also expressed in the eye with possible connections made to the development of eye disease²¹⁻²⁴. Indeed, the application of ACE inhibitors in animal models has been shown to lower IOP^{25,26}. However, whether alterations in the RAS occur in patients developing POAG remains unclear, particularly the relationship between AGT and the pathological development of glaucoma.

Our initial investigations revealed that AGT was expressed in human aqueous humor, with the concentration of ANGII increased in POAG patients compared to normal subjects. Consistent with the results of a prior study²⁴, we detected AGT expression in the primary trabecular meshwork, sclera, and cornea cells. Moreover, we found that ANGII concentrations

were positively correlated with IOP, implying that elevated ANGII levels were involved in the development of glaucoma. On this basis, our study sought to dissect the underlying mechanisms linking ANGII to POAG through the application of *in vitro* and *in vivo* models.

Subsequent analyses showed that treating either transformed human trabecular meshwork cells (HTMCs) or primary HTMCs with ANGII induced transcriptional and protein increases in expression of the fibrosis-related genes *Col1*, *FN* and *α SMA*. In addition, we found that ANGII elevated the levels of intracellular ROS associated with increases in NOX4, with the targeting of NOX4 by gene knockdown or the small molecule inhibitor GLX351322 serving to decrease ROS levels and rescue the fibrotic phenotype induced by ANGII. The application of these findings in a mouse model using periocular conjunctival fornix injections showed that ANGII increased IOP in conjunction with promoting Col1 and FN expression within the trabecular meshwork. Instructively, co-treatment with GLX351322 prevented ANGII-induced rises in IOP while also inhibiting fibrotic gene changes within the trabecular meshwork. Additionally, we found ANGII activates Smad3 in TM cells with the increased Smad3 phosphorylation levels similarly reversed by GLX351322 along with cotreatment using the Smad3 inhibitor SIS3, the latter also alleviating the increased expression of fibrotic genes and rises in IOP. Together this work discloses an association between elevations in ANGII in the aqueous humor, increases in IOP and the development of POAG. Moreover, the elucidation of the mechanistic basis whereby ANGII induces the expression of fibrosis-related genes in the trabecular meshwork through the NOX4-ROS axis with accompany Smad3 signaling activation proposes potentially actionable opportunities for the treatment of glaucoma.

Materials and Methods

Human Trabecular Meshwork Cell Culture

Immortalized (SV40-transformed) HTMCs were purchased from iCell Bioscience Inc. (Shanghai, China), with the cells derived from primary human trabecular meshwork cells (ScienCell Research Laboratories, Catalog Number 6590; Lot Number 16930; CA Number 0002981), and maintained in Dulbecco's modified eagle medium (DMEM)/F12 medium (CD0001, SparkJade, China) supplemented with 15% fetal bovine serum, 100 U/mL penicillin, 100 mg/mL streptomycin. Alternatively, primary trabecular meshwork cells were derived from human eye specimens after enucleation surgery. Briefly, the trabecular meshwork tissue was dissected under a microscope before digestion using the tissue dissociation kit (130-101-540, Miltenyi Biotec, Teterow, Germany) for 2 h. The cells released after digestion were gently passed through a micropipette several times before transfer to culture dishes with the adherent

primary trabecular meshwork cells maintained as for the transformed HTMCs. All experiments were performed on transformed HTMCs with five to seven passages while primary TM cells collected from two separate donors were utilized with five to eight passages²⁷. Human eye collection was approved by the Medical Ethical Committee of Henan Eye Hospital (HNEECKY-2022(18)).

Pharmacological Agents

Where indicated, cells were treated with ANGII (100 nM, HY-13948, MedChemExpress, China) for 48 h alone or in combination with inhibitors targeting NOX4 (GLX351322; 10 μ M, HY-100111, MedChemExpress, China), ROS (NAC; 40 μ M, HY-B0215, MedChemExpress, China), or pSmad3 (SIS3; 100 nM, HY-100444, MedChemExpress, China). Stocks of all agents were prepared in dimethyl sulfoxide (DMSO) with control groups treated with an equal amount of DMSO (1 μ l DMSO in 1 ml medium).

ELISA Assay

Aqueous humor samples collected without blood contamination were subjected to ANGII measurements performed by ELISA assays according to the manufacturer's recommendations (mibio, China). Aqueous humor collection was approved by the Medical Ethical Committee of Henan Eye Hospital (HNEECKY-2022(18)).

Western Blot

Protein concentrations of aqueous humor samples were measured by the bicinchoninic acid (BCA) method using bovine serum albumin (BSA) as the protein standard (Beyotime, P0010S, China). Equal protein amounts were then diluted in 2 \times sodium dodecyl sulfate (SDS) loading buffer and boiled for 10 min. Cells lysates were generated by lysing the cells with a radioimmunoprecipitation assay (RIPA) buffer (Beyotime, P0013B, China) supplemented with a protease inhibitor cocktail (Beyotime, P1049, China) with the lysates then clarified by centrifugation (14,000 \times g \times 10 min at 4°C). A total of 10 μ g of protein/sample was electrophoresed on hand cast 12% SDS-polyacrylamide gel electrophoresis (PAGE) gels using SparkJade kit reagents (Jinan, China) before transfer to nitrocellulose membranes. Protein loading and transfer was validated by Ponceau S staining before subsequent incubation of the membranes with blocking buffer (4% BSA in TBST) for 1 h at room temperature. Thereafter, membranes were incubated overnight at 4°C with diluted primary antibodies, washed three times with TBST for 20 min and then incubated with horseradish peroxidase (HRP)-conjugated secondary antibodies (Goat Anti-Rabbit IgG, SparkJade, EF0002; Goat Anti-Mouse IgG, SparkJade, EF0001, China) in TBST for 1 h at room temperature. After further washing, the antibody-decorated bands were

visualized using a chemiluminescent substrate (Epizyme ECL PicoLight Substrate, SQ202-1, China) and images recorded using a ChemiDoc MP system (BioRad). Primary antibodies used included GAPDH (Proteintech, 10494-1-AP, China, 1:5000), NOX4 (Proteintech, 14347-1-AP, China, 1:1000), Smad3 (Proteintech, 66516-1-Ig, China, 1:1000), pSmad3 (Cell signaling technology, 9520S, USA, 1:500), Fibronectin (HUABIO, ET1702-25, China, 1:3000), Collagen I (Proteintech, 14695-1-AP, China, 1:2000), and α SMA (Proteintech, 14395-1-AP, China, 1:2000).

Immunofluorescence Staining of Cultured Cells

Cells (2 \times 10⁴) were allowed to attach to glass coverslips in 12 wells plates for 24 h before applying the indicated treatments before brief washing with phosphate buffered saline (PBS) and fixation for 15 min with 4% paraformaldehyde (PFA) in PBS solution. Thereafter, the samples were washed in PBS buffer, permeabilized with 0.5% Triton X-100 in PBS for 15 min, further washed with PBS before blocking with 4% BSA in PBS (0.22 μ m filtered) for 60 min at room temperature. The coverslips were then successively incubated with diluted primary antibodies overnight at 4°C followed by one of the secondary antibodies. Either a Donkey anti Rabbit IgG (H+L) 488 (Jackson ImmunoResearch Inc., 711-545-152), or a Donkey anti Mouse IgG (H+L) Cy3 (Jackson ImmunoResearch Inc., 715-165-150, USA) were incubated for 60 min at room temperature, both diluted in blocking solution. After nuclear counterstaining with DAPI solution (MedChemExpress, HY-D1396, China) for 5 min, the coverslips were mounted onto glass slides and images captured using a Leica DMi8 confocal microscope. The primary antibodies used included those against fibronectin (1:500, HUABIO, ET1702-25, China), collagen I (1:500, Proteintech, 14695-1-AP, China), α SMA (1:500, Proteintech, 14395-1-AP, China), and myocilin (1:500, Santa Cruz Biotechnology, sc-137233, USA).

ROS Assay

Cells seeded on live imaging dishes (Biosharp, BS-20-GJM, China) were first incubated in medium without fetal bovine serum for 10 min before the addition of DCFH-DA probe (diluted 1:1000, Beyotime, S0033S, China) along with Hoechst 33342 (diluted 1:500, Beyotime, C1027, China) for 20 min at 37°C. Thereafter, the cells were washed cells 3 times with 37°C medium before capturing images with a Leica DMi8 confocal microscope using the 488 nm and 405 laser lines.

siRNA Transfection

siRNAs were synthesized by GENERAL BIOL (Chuzhou, Anhui, China). Negative control (si-NC) siRNAs sequences were as follow 5'- : UUCUCCGAACGUGUCACGUTT and

5'-ACGUGACACGUUCGGAGAATT. The human *NOX4* siRNAs sequences were as follows: 5'-GGACAAGA UUUGAAUACAATT-3' and 5'-UUGUAUUCAAAUCU UGUCCTT-3'. Transfections were conducted using the Lipo6000 reagent (Beyotime, China) according to the manufacturer's instructions.

RNA Extraction and qPCR Assays

Total RNA was extracted from trypsinized cell suspensions using the SPARKeasy Cell RNA Kit (SparkJade, China) according to the manufacturer's instructions. After quantitation using a NanoDrop spectrophotometer (Thermo scientific), 1 μ g of total RNA was used as template for reverse transcription according to the PrimeScript RT kit (Takara, RR037A, Japan). The cDNA was then diluted and used as a template for quantitative PCR (qPCR) reactions using the 2 \times SYBR Green qPCR Mix (Spark Jade, AH0104-B, China). Reactions were performed on the Step OnePlus real-time PCR system (Applied Biosystems, USA) and the relative expression levels of the target gene mRNA determined against the GAPDH housekeeping gene control using the 2 $^{-\Delta\Delta C_t}$ method. The primer sequences are as follows:

GAPDH F:GGAGCGAGATCCCTCCAAAAT; R:GGCTGTTGTCATACTTCTCATGG

Coll F: GTTGCTGCTTGCAGTAACCTT; R: AGGGCCAAGTCCAACCTCCTT;

FN F: CGGTGGCTGTCAGTCAAAG; R: AAACCTCGGCTTCCTCCATAA;

α *SMA* F: AAAAGACAGCTACGTGGGTGA; R: GCCATGTCTATCGGGTACTTC;

NOX1 F: TTGTTTGGTTAGGGCTGAATGT; R: GCCAATGTTGACCCAAGGATTTT;

NOX2 F: GGGCTGTTCAATGCTTGTGGCT; R: ACATCTTCTCCTCATCATGGTGC;

NOX3 F: ACCGTGGAGGAGGCAATTAGA; R: TGGTTGCATTAACAGCTATCCC;

NOX4 F: CAGATGTTGGGGCTAGGATTG; R: GAGTGTTCCGGACATGGGTA;

NOX5 F: ACTCAGCAGTTTAAGACCATTGC; R: GGACTCTTTCACATGCAGAGC;

Animal Experiments

Female C57BL/6J mice (8 weeks old) were purchased from GemPharmatech (Nanjing, China). Drugs were injected into periocular conjunctival fornix of one eye using 32G

needles as previously reported²⁸ with mice anesthetized using a small animal gas anesthesia machine (Shenzhen RWD Life Technology Co., Ltd, China). Treatment groups consisted of ANGII alone (1 μ l 0.5 μ M ANGII diluted in physiological saline solution [PSS]) and ANGII plus GLX351322 (ANGII with 1 μ M GLX351322); and ANGII alone (1 μ l 0.5 μ M ANGII diluted in PSS) and ANGII plus SIS3 (ANGII with 1 μ M SIS3). Injections were conducted once a week, and IOP was measured during daylight using a TonoLab rebound tonometer (Icare Finland Type TV02). Four weeks later, mice were humanely sacrificed and the excised eye fixed for later immunostaining. Animal experiments complied with the Association for Research in Vision and Ophthalmology Statement. All animal experiments were approved by Animal Ethics Committee of Zhengzhou University (ZZU-LA20220729).

H&E and Immunofluorescence Staining of Tissue Sections

Mouse eyes were fixed with 4% PFA dissolved in PBS buffer for 2 h at room temperature, dehydrated with graded alcohols (30%–100%), immersed two times in xylene for 15 min and then immersed in paraffin overnight at 65°C before paraffin embedding. Microtome cut sections (5 μ m) were adhered to glass slides, deparaffinized with xylene and rehydrated with graded alcohols (100%–50%) before immersing in pure water for 5 min followed by PBS for 5 min. H&E staining was conducted according to the manufacturer's recommendations (H&E Staining Kit, Solarbio, G1120, China). For immunofluorescence staining, antigen retrieval was conducted by heating sections in 0.1 M sodium citrate buffer inside a pressure cooker for 2.5 min after reaching the boiling point. The sections were then washed in PBS for 5 min followed by blocking with 4%BSA/0.5%TritonX-100/PBS solution for 60 min. Afterwards, primary antibodies were applied overnight at 4°C before washing with PBS and application of secondary antibodies for 60 min at room temperature. All antibodies were diluted in blocking buffer prior to use. Finally, the sections were incubated with DAPI solution for 5 min at room temperature, washed with PBS for 3 times, and coverslips applied with mounting medium.

Statistical Analysis

Analyses were performed with GraphPad Prism version 7.0. Age differences between POAG and cataract patients were analyzed with Wilcoxon rank sum test, and patients gender analyzed with the chi-square test. All results are presented as mean \pm SD of at least three independent experiments. Data were determined by unpaired student's *t*-test (2 groups comparison), or one-way analysis of variance (ANOVA; 3 or more group comparisons). *P* < 0.05 was considered as statistically significant.

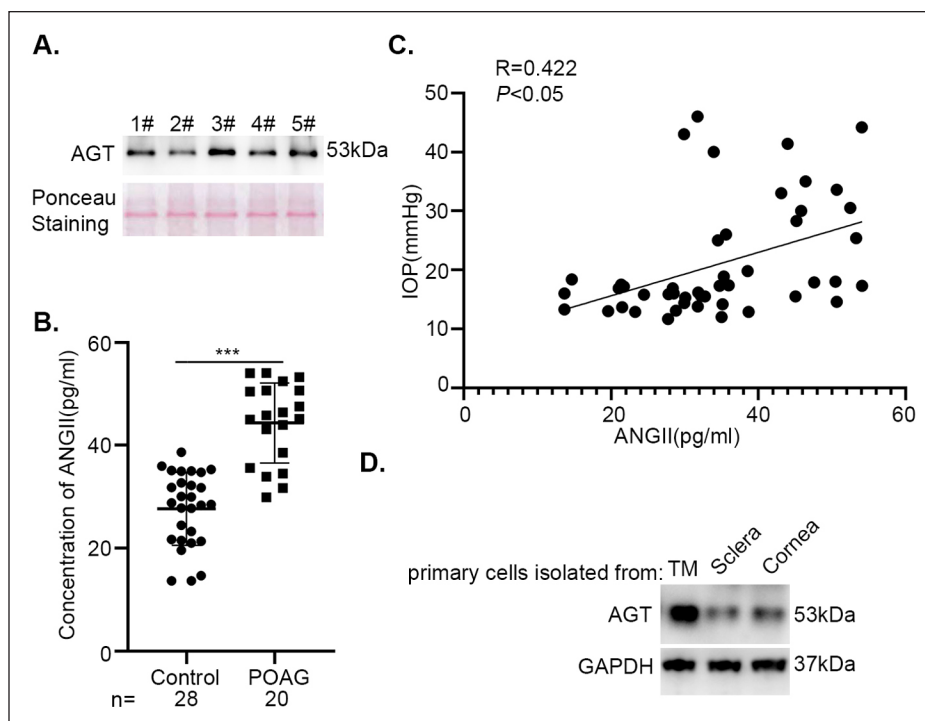


Figure 1. ANGII concentration is elevated in aqueous humor of POAG patients and positively correlated with intraocular pressure. (A) Western blot detection of AGT in five human aqueous humor samples (top) with loading verified using Ponceau staining (bottom). (B) ELISA-based quantification of ANGII concentrations in aqueous humor samples from control (cataract) patients ($n = 28$) and POAG patients ($n = 20$). (C) Positive correlation between ANGII concentrations and intraocular pressures of the 48 patients from (B). ($R = 0.422$ and $P < 0.05$). (D) Western blot detection of AGT in primary cells isolated from the trabecular meshwork, sclera and cornea using. GAPDH served as loading control. Data shown as mean \pm SD, *** $P < 0.001$, unpaired student's t -test. ELISA: enzyme-linked immunosorbent assay; GAPDH: glyceraldehyde 3-phosphate dehydrogenase; ANGII: angiotensin II; POAG: primary open-angle glaucoma; AGT: angiotensinogen.

Results

ANGII Is Elevated in the Aqueous Humor of POAG Patients and Positively Correlates With Intraocular Pressure

Whether the main effector molecule of the RAS, namely ANGII, is present in aqueous humor and functions in pathological development of POAG remained an open question. To initially resolve this point, we screened five aqueous humor samples collected from cataract patients by Western blotting against AGT (the precursor of ANGII). This analysis showed clear immunoreactivity against a single band, with the major protein band revealed by Ponceau S staining as loading control (Fig. 1A). This suggested that AGT is present in the aqueous humor at relatively high levels. We next extended our analysis to consider the levels of ANGII and, whether its concentration was different in POAG versus normal subjects.

Aqueous humor samples were collected from 28 control and 20 POAG patients and subjected to ELISA assays to measure the concentration of ANGII. Analysis of demographic

variables showed there were no significant differences between the groups regarding age range at both gender (Table 1), but notably, we found significant upregulation of ANGII in POAG patients compared with controls (44.35 ± 60.77 vs 27.67 ± 50.63 pg/ml) (Fig. 1B). Moreover, analysis of the cohort of all 48 participants revealed there was an overall strong correlation between ANGII concentrations and IOP values ($R = 0.422$, and $P < 0.05$; Fig. 1C). These results propose a connection between ANGII levels and IOP regulation with the further intimation that ANGII is involved in the pathological development of POAG.

Lastly, we considered the question as to whether ocular ANGII is derived from circulating plasma diffusing through the blood-eye barrier or alternatively results from local production. Indeed, using Western blotting we detected that AGT was expressed in the sclera and corneal tissues while trabecular meshwork cells expressed considerably higher AGT levels (Fig. 1D). ACE is present within aqueous humor²⁹, raising the strong possibility that ANGII may be generated in the eye, although the range of local tissues responsible for local AGT production needs further investigation.

Table 1. Demographic Features of the Study Population.

	POAG (n = 20)	Con (n = 28)	P
Subgroup proportion (%)	42	58	
Mean ages (SD), years	48 (13.78)	48.14 (11.37)	0.983 [#]
Gender			0.954 ^{##}
Male	16 (80%)	21 (75%)	
Female	4 (20%)	7 (25%)	
Mean IOP (SD), mmHg	29.23 (10.16)	15.14 (2.05)	<0.001*

POAG: primary open-angle glaucoma; Con: Cataract; IOP: intraocular pressure.

[#]No significant difference: $P = 0.983$ for POAG vs. Con (Wilcoxon rank sum test).

^{##}No significant difference: $P = 0.954$ for POAG vs. Con (chi-square test).

*Significant pairwise comparisons: $P < 0.001$ for POAG vs. Con (Unpaired t-test).

ANGII Transcriptionally Upregulates Key Fibrosis-Related Genes in HTMCs

To investigate the proposition that elevated ANGII levels are involved in the development of POAG, we first considered how ANGII influences extracellular matrix accumulation in TM cells, a key pathology associated with elevated IOP. Notably, ANGII has been linked to fibrosis induction in various organs^{30–32}, with reports including bovine trabecular meshwork cells³³, although whether ANGII induces fibrosis in human TM cells was still unclear.

Toward determining this question, we employed both immortalized (SV40-transformed) and primary HTMCs prepared in-house. We first confirmed the expression of the key TM cell marker myocilin increased upon DEX treatment²⁷ in both cell line models using immunofluorescence assays (Supplementary Figure 1). Thereafter, we treated human HTMCs were treated for 48 h with ANGII (100 nM) or vehicle control (DMSO) before detection of fibrosis-related proteins using Western blotting. Supporting the notion that ANGII induces fibrosis, we detected significant upregulation of the extracellular matrix proteins Col1 and FN, and the cytoskeletal protein α SMA in both transformed HTMCs and primary HTMCs following ANGII treatment (Fig. 2A, B). Consistently, parallel immunofluorescence staining assays revealed strong increases in Col1, FN, and α SMA staining after ANGII treatment, with quantitative assessment of three independent experiments showing significant increases in the intensity of expression of all three markers (Fig. 2C–F). Similarly, analysis of the Col1 and FN staining as the percentage of positive cells showed significant increases in transformed and primary HTMCs after ANGII treatment (Supplementary Figure 2). Thereafter, to determine whether such increases were transcriptional or post-transcriptional in nature, we examined the respective mRNA levels of these genes using qPCR. Similarly, we observed that ANGII treatment resulted in significantly upregulated levels of *Col1*, *FN*, and *α SMA* mRNA in both transformed HTMCs and primary HTMCs (Fig. 2G, H).

Based on these data, it could be concluded that ANGII transcriptionally upregulates the expression of key fibrosis-related

proteins in HTMCs, thereby promoting defects in TM cells which lead to elevated IOP that in turn, contributes to the development of POAG.

ANGII Increases ROS Levels in HTMCs Through Selective Upregulation of NOX4

While the results above demonstrated that ANGII induces HTMC fibrosis through the transcriptional upregulation of fibrosis-related genes, the upstream signals responsible remained to be determined. It is well known that ANGII increases ROS levels in numerous cell types, and that high ROS levels cause fibrosis^{17,18,32,34}. Thus, we hypothesized that ANGII induced the expression of fibrosis-related genes in HTMCs via increased ROS levels. As before, HTMCs were treated with 100 nM ANGII for 48 h before measuring ROS levels using the DCFH-DA probe. Examination of the resulting signals by confocal microscopy showed that the probe signals were relatively intensified in ANGII treated cells (Fig. 3A) with quantitation from three independent experiments demonstrating that ANGII induces significant upregulation of intracellular ROS levels in both transformed and primary HTMCs (Fig. 3B). Consistently, analyses based on the percentage of DCF-positive cells showed significant increases in both transformed and primary HTMCs after ANGII treatment (Supplementary Figure 3A and B).

NOXs are a small enzyme family whose function involves the production of cytoplasmic ROS³⁵. Consequently, we screened how ANGII treatment affects the expression of *NOX1–5* in HTMCs by qPCR, noting that only *NOX4* was selectively upregulated in transformed HTMCs (Fig. 3C). Further Western blotting analyses confirmed ANGII significantly promoted increases in NOX4 protein in both transformed HTMCs and primary HTMCs (Fig. 3D, E). Then to ascertain whether ANGII caused higher ROS levels through the upregulation NOX4, we implemented transfection studies using RNAi against *NOX4*. Western blotting analysis showed that *NOX4* targeting siRNAs efficiently reduced NOX4 protein levels in ANGII-treated cells to near control levels (Fig. 3F, G). Moreover, the quantitation of overall cellular ROS levels from three independent experiments showed

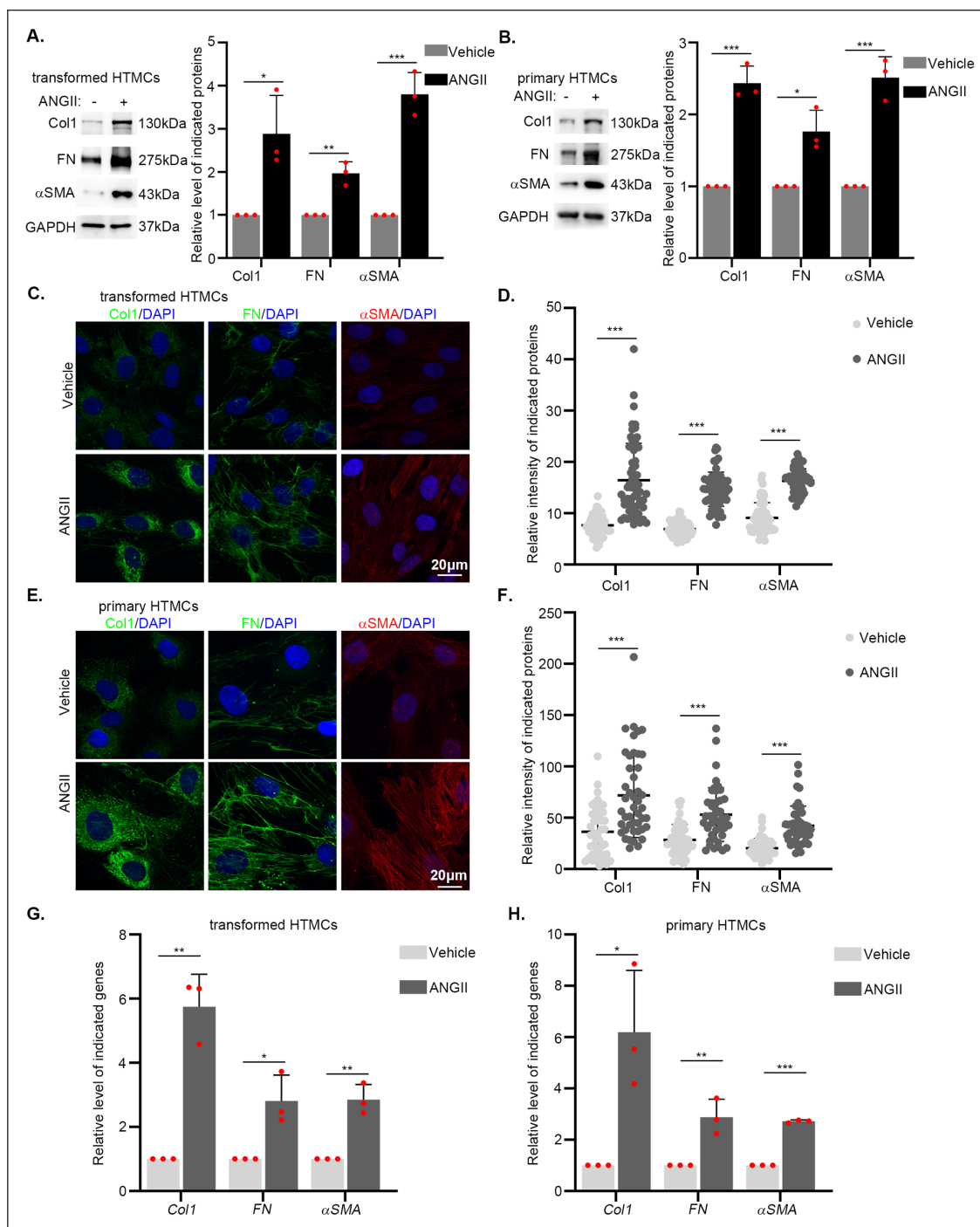


Figure 2. ANGII induces the expression of fibrosis-related genes in HTMCs. (A, B) Transformed (A) and primary HTMCs (B) were treated with or without 100 nM ANGII for 48 h and Western blotting conducted against Col1, FN, and α SMA together with the GAPDH loading control (left). Quantification of ANGII-induced protein changes from three independent experiments (right). (C–F) Representative confocal images of transformed HTMCs (C) and primary HTMCs (E) stained for the indicated fibrosis-related proteins (Col1 (green), FN (green) and α SMA (red)) after treatment with or without 100 nM ANGII for 48 h. Cell nuclei were decorated with DAPI (blue). The resulting intensity values in Col1, FN, and α SMA in transformed HTMCs (D) and primary HTMCs (F) were quantified from three independent experiments ($n = 20$ cells/group for each experiment in (D); $n = 15$ cells in (F)). (G, H) qPCR analysis of transformed (G) and primary HTMCs (H) following treatment with or without 100 nM ANGII for 48 h to detect changes in *Col1*, *FN* and *α SMA* levels. *GAPDH* served as the reference gene with data presented derived from three independent experiments. Data shown are mean \pm SD, * $P < 0.05$; ** $P < 0.01$; *** $P < 0.001$, unpaired student's *t*-test. ANGII: angiotensin II; HTMCs: human trabecular meshwork cells; GAPDH: glyceraldehyde-3-phosphate dehydrogenase; DAPI: 4',6-diamidino-2-phenylindole; qPCR: quantitative PCR.

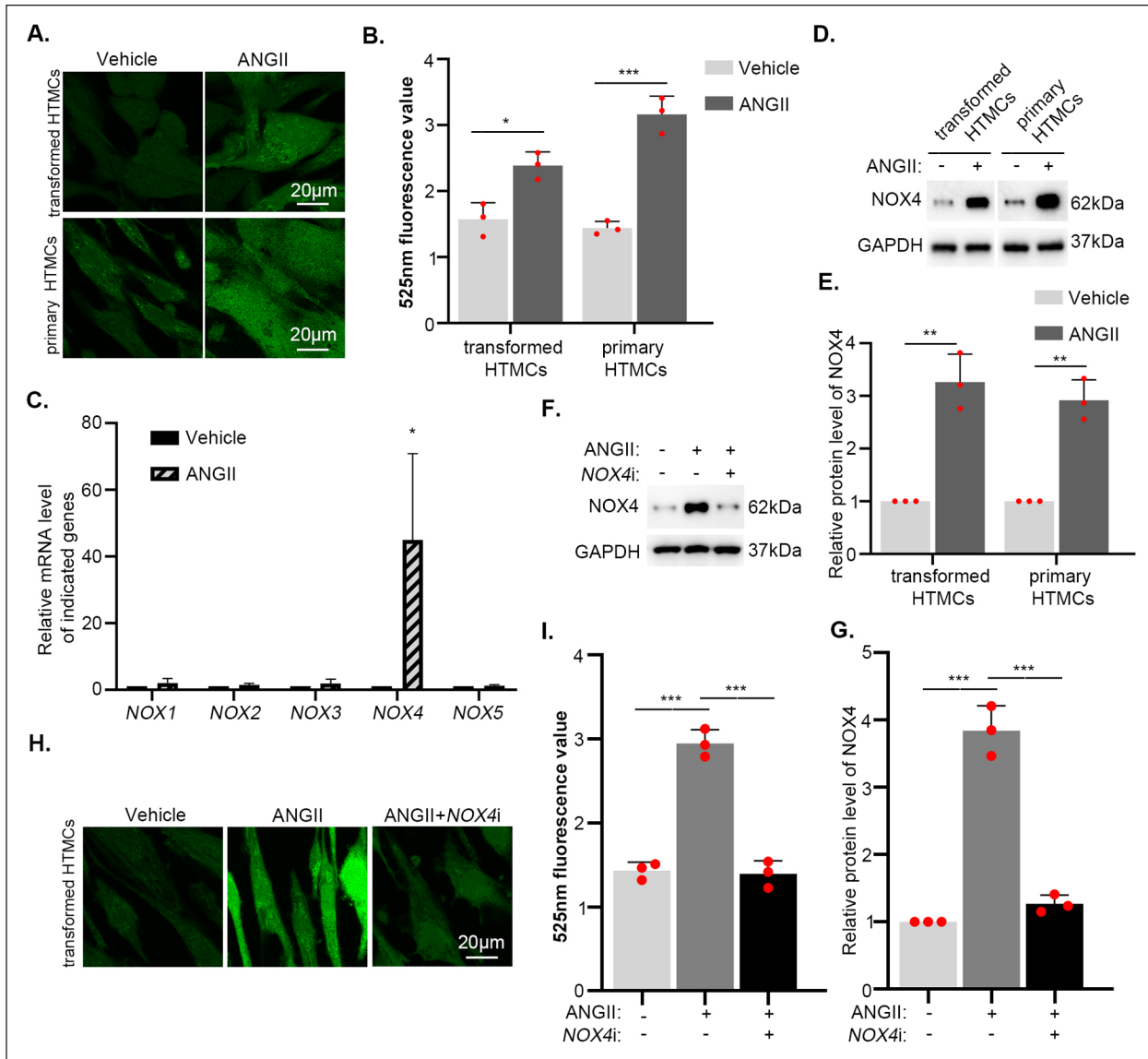


Figure 3. ANGII increases ROS levels of HTMCs through selective upregulation of NOX4. (A, B) Transformed and primary HTMCs were treated with 100 nM ANGII or vehicle (DMSO) for 48 h before measuring ROS levels using DCFH-DA. Representative confocal images (A) and quantitation of ROS levels derived from three independent experiments (B). (C) qPCR analysis of transformed HTMCs following treatment with or without 100 nM ANGII for 48 h measuring *NOX1*, *NOX2*, *NOX3*, *NOX4* and *NOX5* expression. *GAPDH* served as the reference gene with data presented derived from three independent experiments. (D, E) Western blotting analysis of transformed HTMCs and primary HTMCs treated with or without 100nM ANGII for 48 h detecting NOX4 along with GAPDH used as a loading control throughout (D). Quantification from three independent experiments (E). (F, G) Transformed HTMCs were treated for 48 h with vehicle (DMSO), or 100nM ANGII alone and in combination with siRNAs targeting NOX4 (ANGII+NOX4i) before conducting Western blotting analysis against NOX4 (F). Quantification from three independent experiments (G). (H, I) Transformed HTMCs were treated as per (F) before measuring ROS levels using DCFH-DA. Representative confocal images (H) and quantitation of ROS levels from three independent experiments (I). Data shown as mean \pm SD, * $P < 0.05$; ** $P < 0.01$; *** $P < 0.001$, unpaired student's *t*-test (2 groups comparison), or one-way ANOVA (3 or more group comparisons). ANGII: angiotensin II; ROS: reactive oxygen species; HTMC: human trabecular meshwork cells; NOX4: NADPH oxidase 4; DMSO: Dimethyl sulfoxide; DCFH-DA: Dichlorodihydrofluorescein Diacetate; GAPDH: glyceraldehyde-3-phosphate dehydrogenase; qPCR: quantitative PCR; ANOVA: analysis of variance.

that *NOX4* knockdown rescued the induction of elevated ROS levels induced by ANGII treatment (Fig. 3H, I). Moreover, assessing the results based on the percentage of DCF positive cells showed *NOX4* knockdown reversed

elevations in ROS induced by ANGII treatment (Supplementary Figure 3C and D). Thus, the activity of NOX4 underlies the increases in intracellular ROS resulting from ANGII treatment of HTMCs.

ANGII Mediates the Fibrotic Phenotype of HTMCs Via NOX4-Mediated Increases in ROS

High ROS levels promote the expression of fibrosis-related markers in many cell types including HTMCs³⁶ with our preceding results establishing connections between NOX4 and increased ROS levels in response to ANGII. To formalize the connection between NOX4 and the induction of fibrosis-related genes in HTMCs, we examined whether *NOX4* knockdown was able to rescue the phenotype induced by ANGII treatment. Indeed, using Western blotting to compare the relative levels of fibrosis-related proteins, we observed that *NOX4* knockdown in transformed HTMCs reversed the increases in Col1, FN and α SMA induced by ANGII, significantly decreasing their respective expression to control levels (Fig. 4A, B). In support of these findings, immunofluorescence labeling and confocal imaging showed that the high intensity staining of Col1, FN, and α SMA following ANGII treatment was reversed by transfection of *NOX4* siRNAs, with significant decreases confirmed by quantitative image analysis (Fig. 4C, D). Likewise, the percentage of Col1 and FN-positive cells induced by ANGII treatment also was reversed by *NOX4* gene silencing (Supplementary Figure 4). Together these data served to reconcile that the upregulation of NOX4 underlies the ANGII-induced expression of fibrosis-related genes in HTMCs, although it remained to be formally demonstrated that ROS produced by NOX4 was the decisive mediator.

To clarify the role of NOX4 in the ANGII-induced increases in ROS levels, we examined the impact of co-treating HTMCs with the NOX4 inhibitor GLX351322 (10 μ M) or the ROS inhibitor NAC (40 μ M)^{37,38}. Instructively, these experiments showed that treatments with either GLX351322 or NAC effectively decreased the elevation of ROS levels in transformed HTMCs following ANGII treatment assessed by either overall intensity measurements (Fig. 5A, B) or the percentage of DCF-positive cells (Supplementary Figure 5A and B). Moreover, assessment of the fibrosis-related phenotype using Western blotting similarly showed that GLX351322 or NAC treatments significantly dampened ANGII-induced increases in Col1, FN, and α SMA in transformed HTMCs (Fig. 5C, D). Moreover, the results of immunofluorescence staining showed that GLX351322 and NAC all significantly decreased staining intensity increases in Col1, FN, and α SMA in ANGII-treated cells (Fig. 5E, F) as well as decreasing cell positivity for staining against Col1 and FN (Supplementary Figure 5 C and D). These collective experiments therefore reveal that ANGII induces fibrosis in transformed HTMCs via NOX4 generated increases in cellular ROS.

ANGII Induces Fibrotic Gene Expression in HTMCs Via Smad3 Activation

Having established above that ANGII induces fibrosis-related gene expression in HTMCs via NOX4 generated

increases in cellular ROS, we turned to consider what signaling pathway(s) were responsible for driving the expression of the corresponding fibrosis-related genes. Notably, tumor growth factor β (TGF β & Smad3 signaling is the key pathway responsible for promoting HTMC fibrosis with effects mediated through transcriptional upregulation³⁹. Intriguingly, high ROS levels are known to activate Smad3^{40,41}, proposing that ANGII functions in this scenario through activating Smad3. To test this hypothesis, we examined the activation of Smad3 via Western blotting against phosphorylated (p) serine residues in its C-terminus. Strikingly, we observed that ANGII treatment significantly increased pSmad3 level in transformed HTMCs, while not influencing the total levels of Smad3 (Fig. 6A).

To confirm whether the activation of Smad3 by ANGII was dependent on NOX4, we treated transformed HTMCs with ANGII in combination with GLX351322. Notably, Western blotting analyses revealed that NOX4 inhibition efficiently attenuated the increase in pSmad3 levels, along with rescuing the ANGII-induced fibrosis-related phenotype (Fig. 6B). Moreover, as expected, the addition of the Smad3 inhibitor SIS3⁴² significantly suppressed the increases in Smad3 activity induced by ANGII while instructively also rescuing the resulting phenotype (Fig. 6C, D). Of further relevance, we did not see any increase in TGF β 2 production after treating cells with ANGII (data not shown).

These collective data indicate that ANGII increases cellular ROS in HTMC through the upregulation of NOX4 with the concurrent activation Smad3 serving to drive increases in key fibrosis-related proteins.

ANGII Induces the Expression of Fibrosis-Related Genes in Trabecular Meshwork Cells in vivo Through Activation of Nox4 and Smad3

A pertinent question remained as to whether ANGII induces the expression of fibrosis-related genes in trabecular meshwork cells in *in vivo*? Toward an answer, we adopted the findings gleaned from our *in vitro* experiments to examine the contribution of ANGII to POAG pathogenesis in a murine model. Moreover, we included the application of pharmacological inhibitors to dissect out the responsible pathways and to discern possible treatment strategies.

We first established a murine model based on injections into the periocular conjunctival fornix²⁸. Accordingly, injections were performed with physiological salt solutions containing vehicle (vehicle control), ANGII alone or in combination with the Nox4 inhibitor GLX351322 (Fig. 7A). IOP measurements confirmed that ANGII treatment increased IOP compared to control group mice, with these increases partially rescued by cotreatment with GLX351322 (Fig. 7B). Furthermore, examination of eye sections using immunostaining showed that ANGII treatment increased the intensity of staining against Col1 and FN in trabecular meshwork cells, which was rescued by GLX351322 treatment (Fig. 7C–F and Supplementary Figure 6). Thus, the actions of ANGII

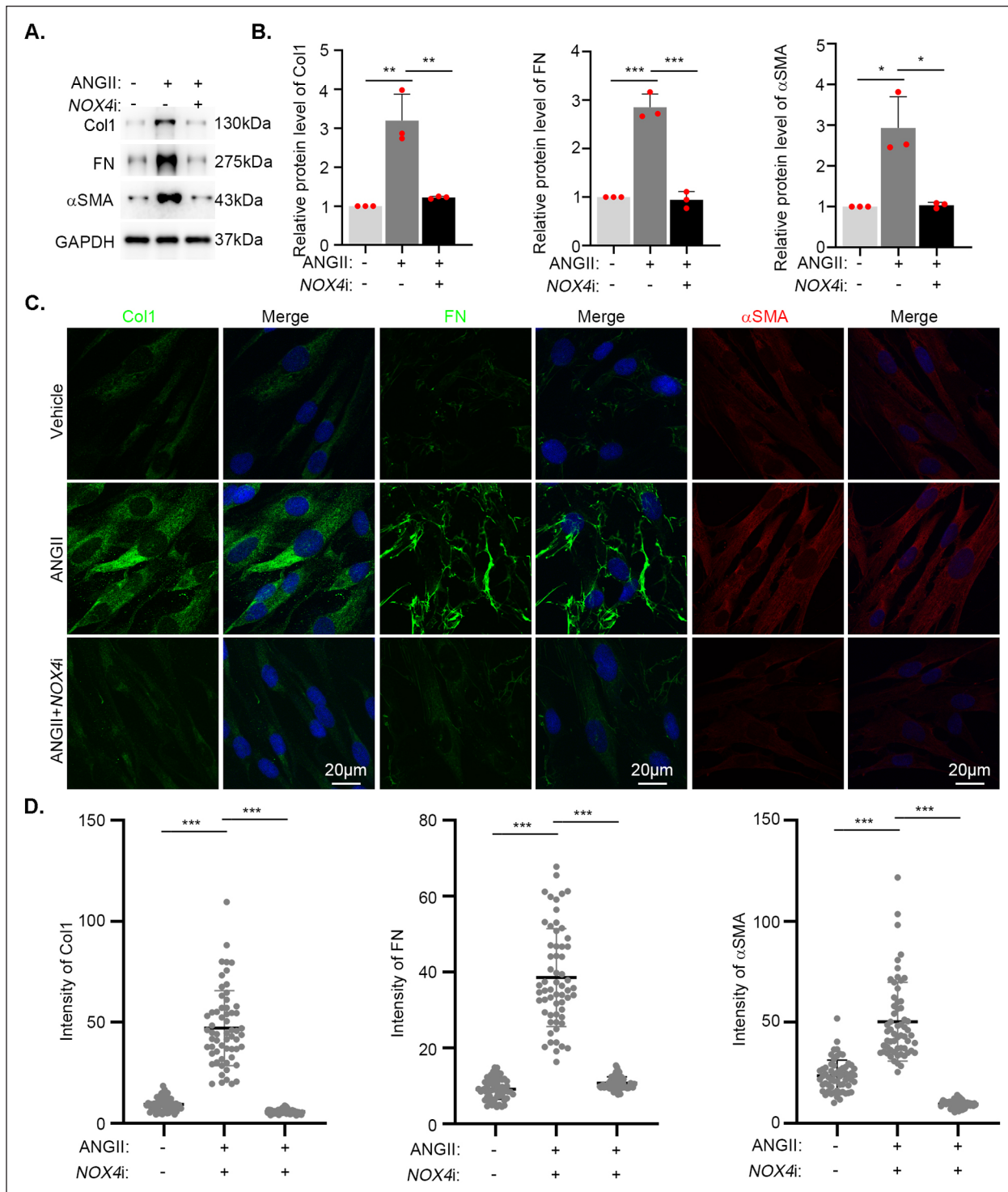


Figure 4. Knockdown of *NOX4* rescues the elevated expression of fibrosis-related genes induced by ANGII. (A, B) Transformed HTMCs were treated with vehicle (DMSO), 100nM ANGII or ANGII+*NOX4* siRNA for 48 h before conducting Western blotting analyses against Col1, FN and αSMA (A). GAPDH was used as a loading control throughout with (B) showing quantification from three independent experiments. (C, D) Representative confocal images of transformed HTMCs stained with the indicated proteins (Col1 (green), FN (green) and αSMA (red)) (C) after treatment as per (A). Cell nuclei were decorated with DAPI (blue) with the intensity of Col1, FN and αSMA staining (D) quantified from three independent experiments ($n = 20$ cells/group for each experiment). Data show as mean \pm SD, ** $P < 0.01$; *** $P < 0.001$, unpaired student's *t*-test (2 groups comparison), or one-way ANOVA (3 or more group comparisons). ANGII: angiotensin II; HTMC: human trabecular meshwork cells; *NOX4*: NADPH oxidase 4; DMSO: Dimethyl sulfoxide; GAPDH: glyceraldehyde-3-phosphate dehydrogenase; DAPI: 4',6-diamidino-2-phenylindol; ANOVA: analysis of variance.

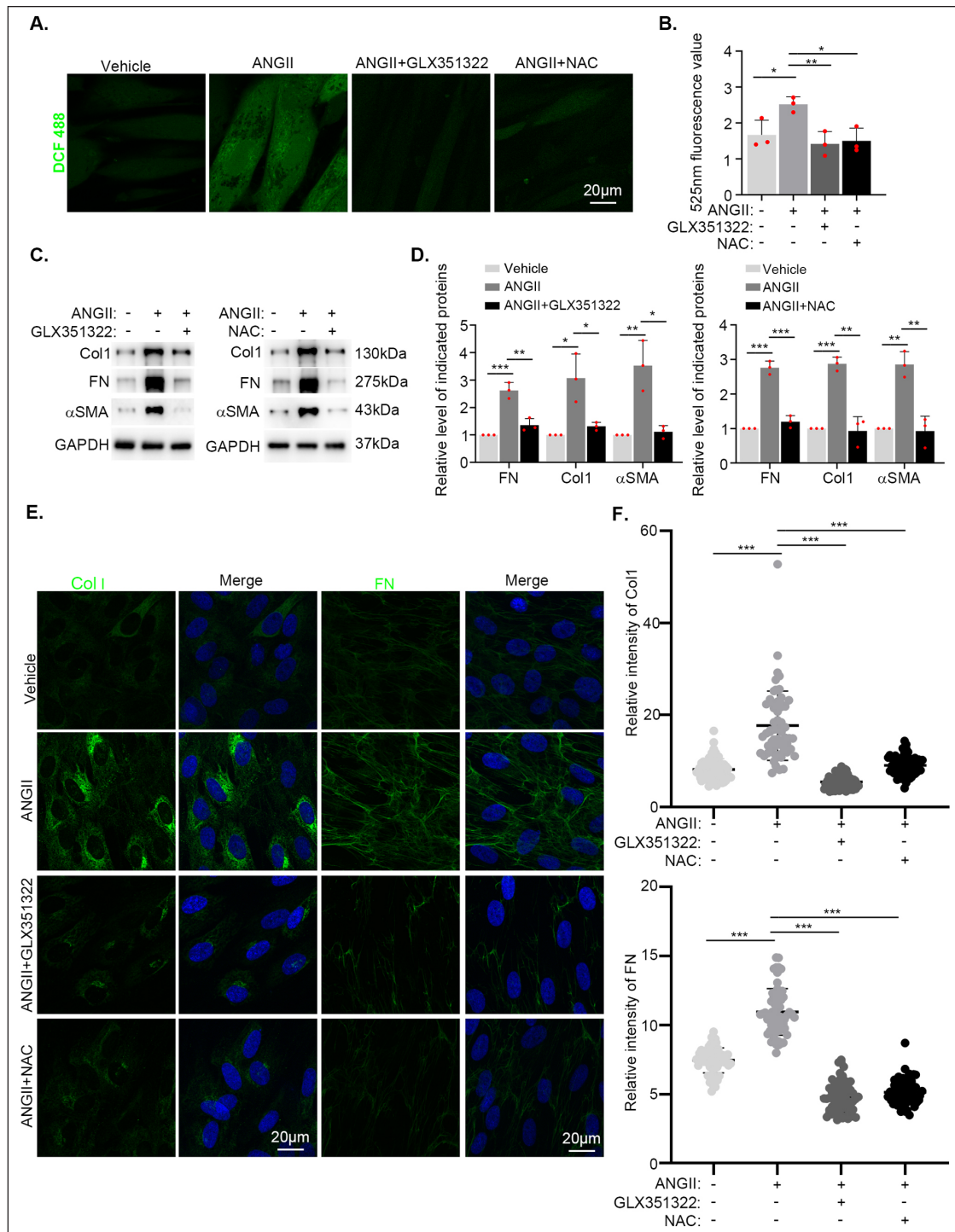


Figure 5. Pharmacological inhibition of NOX4 and ROS alleviates the fibrosis-related changes in HTMCs induced by ANGII. (A, B) Transformed HTMCs were treated for 48 h with vehicle (DMSO) or 100 nM ANGII alone or in combination with the indicated inhibitors targeting NOX4 (GLX351322; 10 μM) or the ROS scavenger NAC (40 μM) before detecting cellular ROS levels with DCFH-DA. Representative confocal images (A) with quantitation from three independent experiments shown in (B). (C, D) Parallel Western blotting experiments were performed on the cells in (A) to detect the levels of Col1, FN and αSMA (C). GAPDH was used as a loading control throughout. (D) shows quantification from three independent experiments. (E, F) Parallel immunostaining and confocal imaging was performed on the cells in (A) to detect the expression of Col1 (green), FN (green) and αSMA (red) along with nuclear counterstaining with DAPI (blue). Representative confocal images (E) with intensity quantification from three independent experiments (F) using $n = 20$ cells/group for each experiment. Data shown as mean \pm SD, * $P < 0.05$; ** $P < 0.01$; *** $P < 0.001$, unpaired student's t -test (2 groups comparison), or one-way ANOVA (3 or more group comparisons). ROS: reactive oxygen species; HTMC: human trabecular meshwork cells; ANGII: angiotensin II; NOX4: NADPH oxidase 4; DMSO: Dimethyl sulfoxide; DCFH-DA: Dichlorodihydrofluorescein Diacetate; GAPDH: glyceraldehyde-3-phosphate dehydrogenase; DAPI: 4',6-diamidino-2-phenylindole; ANOVA: analysis of variance.

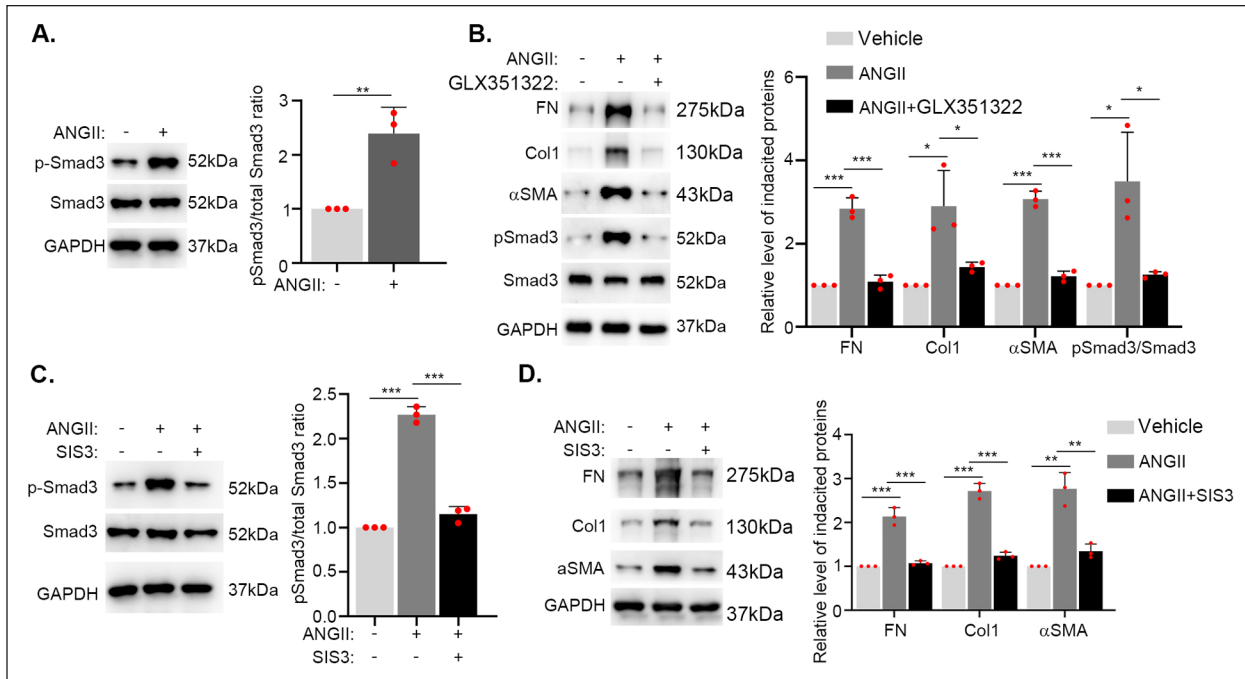


Figure 6. ANGII induces fibrosis-related gene expression in HTMCs via Smad3 activation. (A) Transformed HTMCs were treated with vehicle (DMSO) or 100nM ANGII for 48h before conducting Western blotting against phosphorylated (pSmad3) and total Smad3 (left). GAPDH served as a loading control throughout. The Smad3/pSmad3 ratio was quantified from three independent experiments (right). (B) Transformed HTMCs were treated for 48h with DMSO, ANGII or ANGII combined with GLX351322 (ANGII+GLX351322) before Western blotting against Col1, FN, αSMA, total Smad3 and pSmad3 (left). Quantification from three independent experiments (right). (C, D) Transformed HTMCs were treated for 48h with DMSO, ANGII or ANGII combined with SIS3 (ANGII+SIS3) before Western blotting against total Smad3 and pSmad3 (C; left) or Col1, FN and αSMA (D; left). The Smad3/pSmad3 ratio (C; right) or Col1, FN and αSMA levels (D; right) were quantified from three independent experiments. Data shown as mean ± SD, * $P < 0.05$; ** $P < 0.01$; *** $P < 0.001$, unpaired student's *t*-test (2 groups comparison), or one-way ANOVA (3 or more group comparisons). ANGII: angiotensin II; HTMC: human trabecular meshwork cells; DMSO: Dimethyl sulfoxide; ANOVA: analysis of variance.

against HTMCs are phenocopied in a murine model with Nox4 shown to be similarly essential for invoking fibrosis in the TM.

We then also sought to clarify whether Smad3 activation was similarly pertinent for the outcomes in the *in vivo* model. Accordingly, periocular conjunctival fornix injections were conducted with ANGII alone or in combination with SIS3 along with physiological saline controls (Fig. 8A). Importantly, the elevated IOP measurements observed in ANGII treated mice were partially alleviated by SIS3 (Fig. 8B). Consistently, immunostaining of eye sections showed that the increased intensity of Col1 and FN staining in the trabecular meshwork caused by ANGII treatment was also rescued by SIS3 treatment (Fig. 8C–F).

Thus, our collective data propose a working model whereby ANGII increases intracellular ROS levels through the upregulation of NOX4 with pursuant activation of Smad3. In turn, the latter promotes transcriptional increases in fibrosis-related genes, leading to fibrosis-related defects and the aberrant function of TM cells, thereby elevating IOP (Fig. 9).

Discussion

Over the past decades, the presence of local RASs has been revealed in various tissues with the accompanying discovery that angiotensin II (ANGII) acts as a novel immunomodulator and profibrotic molecule^{12–16,19}. In accordance, the hypothesis that a localized RAS contributes to eye homeostasis has been prominent²³. Nonetheless, the details of the function of the RAS and its role in disease are poorly understood, largely due to a lack of direct experimental evidence. Notably, whether the key RAS component ANGII functions in the development of glaucoma is also unclear. Here, we detected AGT in aqueous humor with its expression in eye derived primary cells suggesting local production, together supporting the notion that the eye has a localized RAS^{22–24}. However, the notion that the source of AGT in aqueous humor involves local production within the eye needs further study. Notwithstanding this point, the concentration increases of ANGII in the aqueous humor of POAG patients and its positive correlation with IOP provides a clear indication that a pathological association exists between ANGII and POAG.

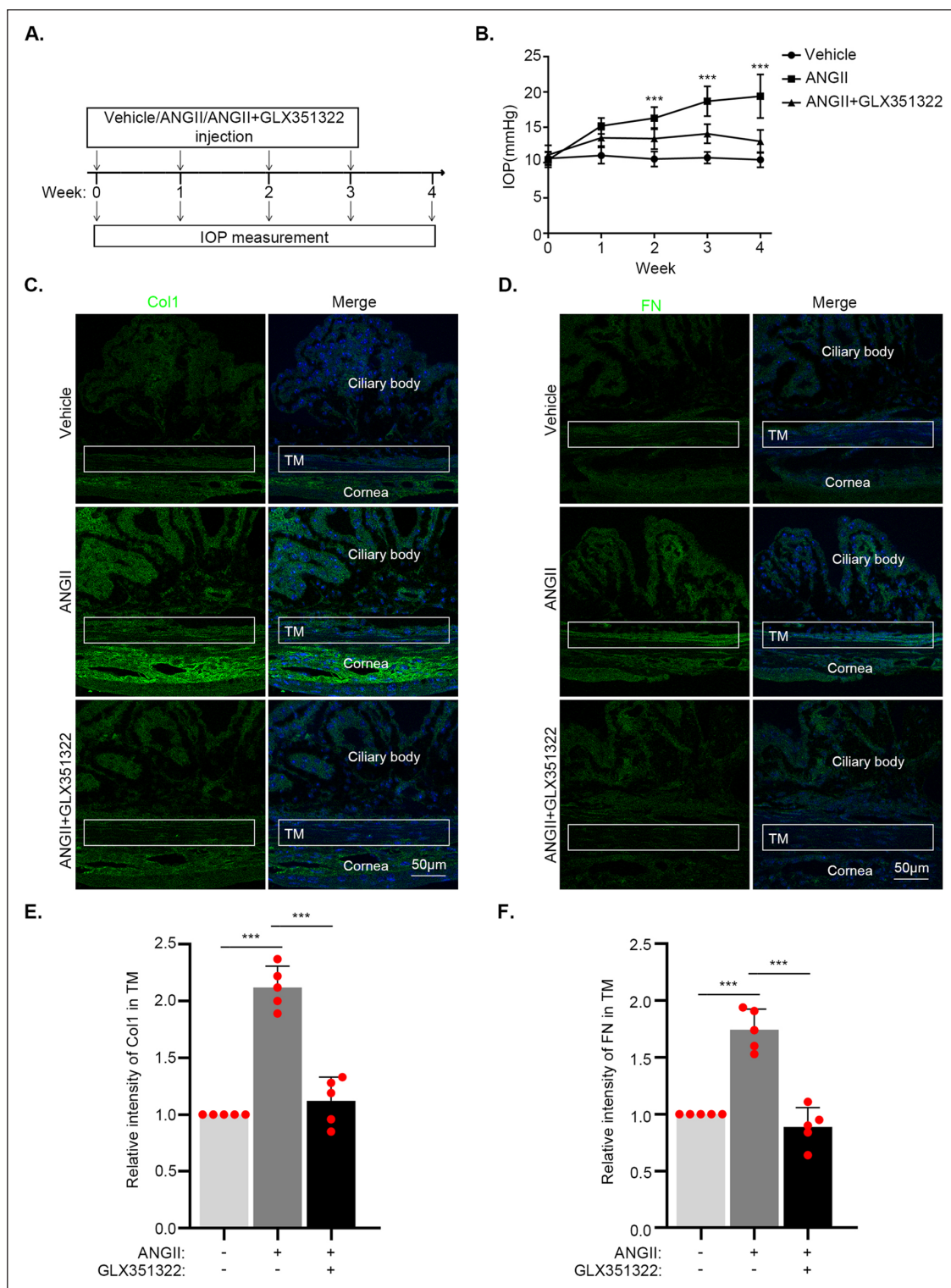


Figure 7. Inhibition of NOX4 rescues elevations in IOP and the expression of fibrosis-related genes of the trabecular meshwork induced by ANGII *in vivo*. (A, B) An *in vivo* mouse model was established by injecting ANGII alone or in combination with the NOX4 inhibitor GLX351322 into the periocular conjunctival fornix once a week (A). The IOPs of the mice were measured every week (B) ($n = 10$ mice/group). (C–F) Representative confocal images of one eye section from the treatment groups in (A) showing immunostaining against Col1 (C; green) and FN (D; green) with cell nuclei decorated with DAPI (blue). The relative intensities of Col1 (E) and FN (F) staining were quantified in TM tissues denoted by the boxed area indicating the trabecular meshwork (TM). Data were derived from 5 individual eyes representing all animals from each treatment group. Data shown as mean \pm SD, *** $P < 0.001$, unpaired student's *t*-test (2 groups comparison), or one-way ANOVA (3 or more group comparisons). IOP: intraocular pressure; ANGII: angiotensin II; TM: trabecular meshwork; NOX4: NADPH oxidase 4; ANOVA: analysis of variance.

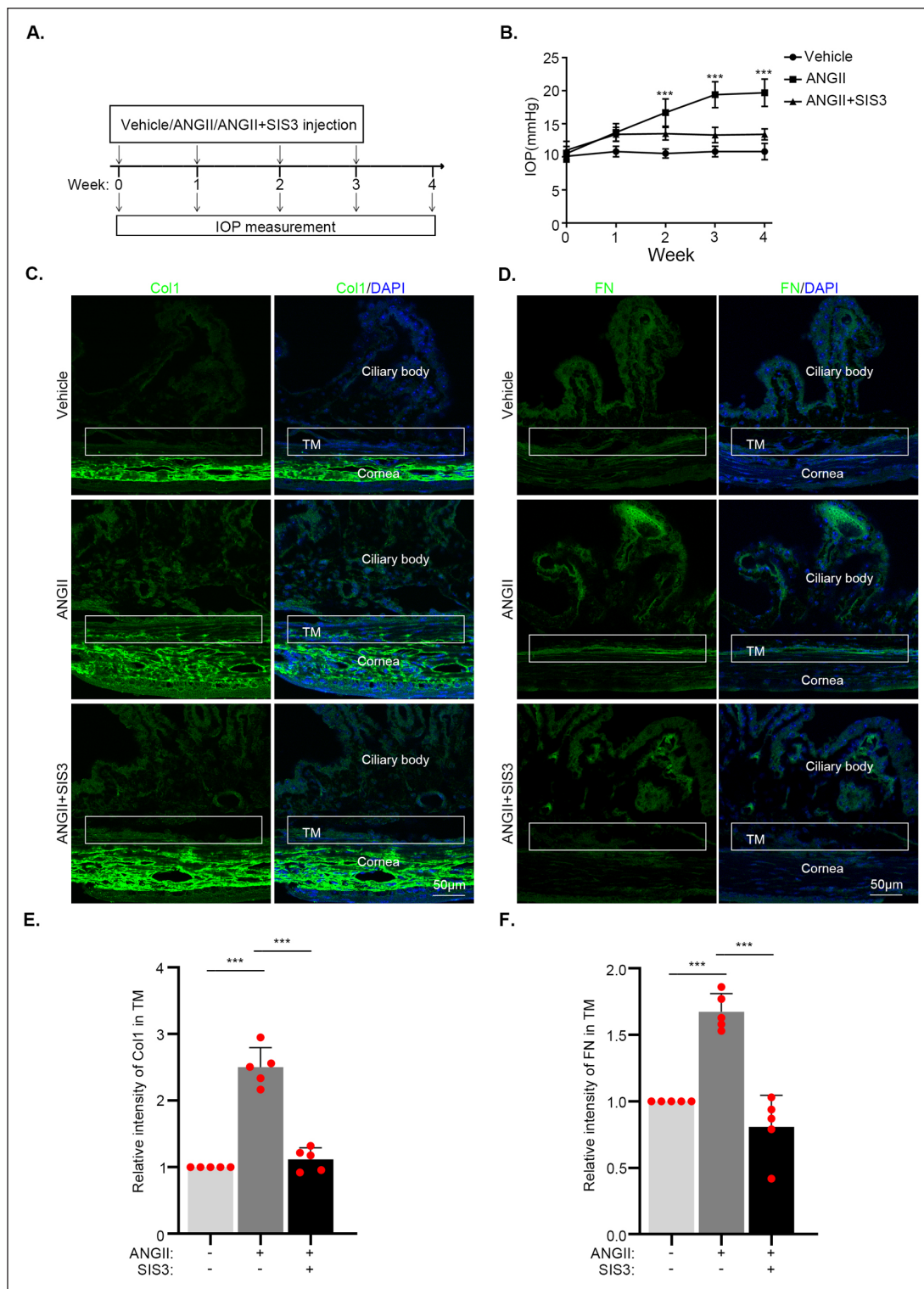


Figure 8. Inhibition of Smad3 rescues the expression of fibrosis-related genes induced by ANGII *in vivo*. (A, B) An *in vivo* mouse model was established by injecting ANGII alone or in combination with the Smad3 inhibitor SIS3 into the periocular conjunctival fornix once a week (A). The IOPs of the mice were measured every week (B) ($n = 10$ mice/group). (C–F) Representative confocal images of one eye section from the treatment groups in (A) showing immunostaining against Col1 (C; green) and FN (D; green) with cell nuclei decorated with DAPI (blue). The relative intensities of Col1 (E) and FN (F) staining were quantified in TM tissues denoted by the boxed area indicating the trabecular meshwork (TM). Data were derived from 5 individual eyes representing all animals from each treatment group. Data shown as mean \pm SD, *** $P < 0.001$, unpaired student's *t*-test (2 groups comparison), or one-way ANOVA (3 or more group comparisons). ANGII: angiotensin II; IOP: intraocular pressure; TM: trabecular meshwork; DAPI: 4',6-diamidino-2-phenylindole; ANOVA: analysis of variance.

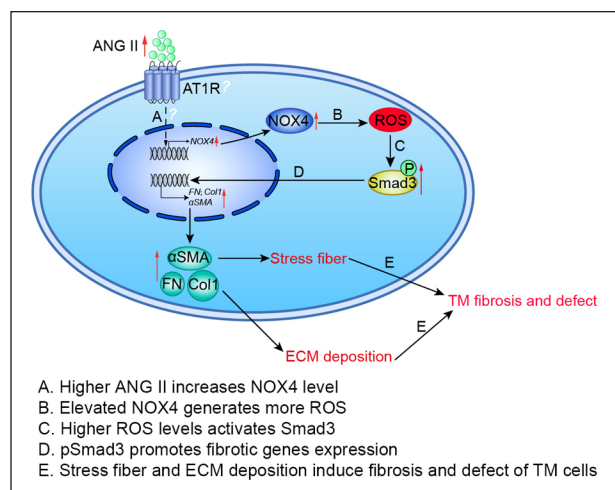


Figure 9. Working molecular model. Elevated ANGII concentrations in the aqueous humor of patients with POAG serve to increase NOX4 levels to generate higher ROS levels in TM cells (A, B). In turn, elevations in ROS activate Smad3 to promote fibrotic gene expression (C, D) with resulting stress fiber/ECM deposition to induce fibrotic defects in TM cells (E). ANGII: angiotensin II; POAG: primary open-angle glaucoma; ROS: reactive oxygen species; TM: trabecular meshwork; NOX4: NADPH oxidase 4; ECM: extracellular matrix.

Following on from these findings, we addressed the hypothesis that increases in ANGII concentrations in the eye are involved in the development of glaucoma. Our study focused on modeling the pathological functions of elevated ANGII, establishing that ANGII promotes the expression of fibrosis-related genes of TM cells through increases in cellular ROS levels driven by the upregulation of NOX4 along with the activation of Smad3. AT1R is the major receptor of ANGII, which belongs to the B family of the G protein-coupled receptor (GPCR) family, and AT1R mediates most of the known effects of ANGII^{43,44}. Indeed, excessive activation of AT1R through ANGII binding is the root cause of certain pathological processes, most notably hypertension where treatment with AT1R inhibitors can effectively reverse high blood pressure. And intriguingly, such inhibitors also serve to depress IOP, again providing evidence of the importance of the localized RAS in the eye together with a role for ANGII in maintaining IOP⁴⁵. However, further study is needed to decipher how ANGII upregulates NOX4, and, also whether the effects of ANGII on TM cells are similarly dependent upon AT1R signaling.

Our study also serves to reconcile some disparate points in the current literature. First, it is known that high levels of ROS in human trabecular network cells and vascular smooth muscle cells induce fibrosis through the activation of Smad3^{36,41}. Here we connected the ANGII-mediated increases in ROS levels and the resulting upregulation of fibrosis-related genes of TM cells with the involvement of

Smad3 signaling. Instructively, Smad3 activation appeared to occur independently of increased TGF β 2 levels thereby suggesting the actions of ANGII were predominantly caused through altered ROS levels. However, whether the increases in ROS levels in TM cells occur through ROS production by mitochondria as previously found^{46,47} remains to be determined. Second, the TGF β /Smad3 pathway is known to induce ROS through promoting NOX4 expression^{48,49}, with our results showing this mechanism can also be invoked by ANGII, and further proposing that ROS and activated Smad3 constitute key elements of a regulatory loop that drives fibrosis. Importantly, from a clinical perspective, we found that the inhibition of NOX4 along with Smad3 activation with SIS3 rescues the fibrotic phenotype of TM cells *in vitro* and *in vivo*. Additionally, the same treatments were at least partially effective in preventing the elevation of IOP induced by ANGII treatment, suggesting potential opportunities to explore as preventative strategies. Notably, we did not directly measure if ANGII was delivered to the trabecular meshwork. However, our experimental outcomes suggest specific actions against the TM, although we cannot discount effects on other eye tissues. Similarly, the presumed mechanism involved in the periocular transfer of the ANGII peptide remains unclear although certain peptides have been shown to permeate the eye through similar route⁵⁰. Consequently, more work is needed to evaluate the utility of periocular delivery of different peptides and drugs.

Lastly, while our study focused on mechanisms connecting ANGII with the fibrosis of TM cells, it must be considered that the ANGII/NOX/ROS axis is known to be involved in pathological effects in other organs besides fibrosis, including inflammation¹⁹ and ROS-mediated senescence^{20,51,52}. Indeed, there is increasing appreciation in many chronic diseases that senescence may be intrinsically linked to both inflammation and fibrosis. Senescent cells are renowned for their secretion of proinflammatory mediators together with various factors capable of modifying the extracellular matrix, otherwise known as the senescence-associated secretory phenotype (SASP)⁵³. The SASP is a likely culprit in the development of fibrosis⁵⁴. But whether the effects of elevated ANGII extend to the induction of senescence in TM cells remains to be determined in future studies.

Acknowledgment

The Authors appreciate the Reviewers' time and efforts to improve the quality and clarity of our study.

Authors' Contributions

Haijun Li and Shichao Duan conceived and designed the experiments. Shichao Duan, Haijun Li, Huiling Cui, Jing Ren, Di Wang, Rumeng Zhao, Shichao Zhu, Siqing Liu, Xiaohui Liu, Shuai Tian, Yuanyuan Zhang, Panpan Zhao performed the experiments. Haijun Li and Shichao Duan analyzed the data. Shichao Duan, Haijun Li, Rick F. Thorne and Peng Li wrote the paper.

Availability of Data and Material

All data generated or analyzed during this study are included in the main text and the supplementary information files.

Ethical Approval

Ethical approval to report this case series was obtained from the Medical Ethical Committee of Henan Eye Hospital (HNEECKY-2022(18)).

Statement of Human and Animal Rights

All procedures in this study were conducted in accordance with the Association for Research in Vision and Ophthalmology Statement and Animal Ethics Committee of Zhengzhou University (ZZU-LA20220729) approved protocols.

Statement of Informed Consent

Written informed consent was obtained from the patient(s) for their anonymized information to be published in this article.

Declaration of Conflicting Interests

The author(s) declared no potential conflicts of interest with respect to the research, authorship, and/or publication of this article.

Funding

The author(s) disclosed receipt of the following financial support for the research, authorship, and/or publication of this article: This work was supported by the National Natural Science Foundation of China [U1904166]; Henan Medical Science and technology research plan [SBGJ2018072].

ORCID iDs

Peng Li  <https://orcid.org/0000-0001-8262-7330>

Shichao Duan  <https://orcid.org/0000-0002-3177-4194>

Supplemental Material

Supplemental material for this article is available online.

References

- Quigley HA, Broman AT. The number of people with glaucoma worldwide in 2010 and 2020. *Br J Ophthalmol*. 2006;90(3):262–67.
- McMonnies CW. Glaucoma history and risk factors. *J Optom*. 2017;10(2):71–78.
- Tham YC, Li X, Wong TY, Quigley HA, Aung T, Cheng CY. Global prevalence of glaucoma and projections of glaucoma burden through 2040: a systematic review and meta-analysis. *Ophthalmology*. 2014;121(11):2081–90.
- Goel M, Picciani RG, Lee RK, Bhattacharya SK. Aqueous humor dynamics: a review. *Open Ophthalmol J*. 2010;4:52–59.
- Kaeslin MA, Killer HE, Fuhrer CA, Zeleny N, Huber AR, Neutzner A. Changes to the aqueous humor proteome during glaucoma. *PLoS ONE*. 2016;11(10): e0165314.
- Cumurcu T, Bulut Y, Demir HD, Yenisehirli G. Aqueous humor erythropoietin levels in patients with primary open-angle glaucoma. *J Glaucoma*. 2007;16(8):645–48.
- Xue M, Ke Y, Ren X, Zhou L, Liu J, Zhang X, Shao X, Li X. Proteomic analysis of aqueous humor in patients with pathologic myopia. *J Proteomics*. 2021;234:104088.
- Cho MC, Kim RB, Ahn JY, Yoo WS, Kim SJ. Aqueous humor and serum 25-Hydroxyvitamin D levels in patients with cataracts. *BMC Ophthalmol*. 2020;20(1):6.
- Balbaba M, Ulaş F, Erdağ M, Yıldırım H, Çeliker Ü, Aydın S. Evaluation of aqueous humor and serum cortistatin levels in diabetic patients with and without diabetic retinopathy. *Eur J Ophthalmol*. 2021;31(2):638–42.
- Mimura T, Funatsu H, Noma H, Shimura M, Kamei Y, Yoshida M, Kondo A, Watanabe E, Mizota A. Aqueous humor levels of cytokines in patients with age-related macular degeneration. *Ophthalmologica*. 2019;241(2):81–89.
- Te Riet L, van Esch JH, Roks AJ, van den Meiracker AH, Danser AH. Hypertension: renin-angiotensin-aldosterone system alterations. *Circ Res*. 2015;116(6):960–75.
- Kurdi M, De Mello WC, Booz GW. Working outside the system: an update on the unconventional behavior of the renin-angiotensin system components. *Int J Biochem Cell Biol*. 2005;37(7):1357–67.
- Meng Y, Li T, Zhou GS, Chen Y, Yu CH, Pang MX, Li W, Li Y, Zhang WY, Li X. The angiotensin-converting enzyme 2/angiotensin (1-7)/Mas axis protects against lung fibroblast migration and lung fibrosis by inhibiting the NOX4-derived ROS-mediated RhoA/Rho kinase pathway. *Antioxid Redox Signal*. 2015;22(3):241–58.
- Sachse A, Wolf G. Angiotensin II-induced reactive oxygen species and the kidney. *J Am Soc Nephrol*. 2007;18(9):2439–46.
- Zhang Y, Liu H, Jia W, Qi J, Zhang W, Zhang W, Liang G, Zhang Y, Chen AH. Myeloid differentiation protein 2 mediates angiotensin ii-induced liver inflammation and fibrosis in mice. *Molecules*. 2019;25(1):25.
- Cabello-Verrugio C, Córdova G, Salas JD. Angiotensin II: role in skeletal muscle atrophy. *Curr Protein Pept Sci*. 2012;13(6):560–69.
- Zheng J, Li G, Chen S, Bihl J, Buck J, Zhu Y, Xia H, Lazartigues E, Chen Y, Olson JE. Activation of the ACE2/Ang-(1-7)/Mas pathway reduces oxygen-glucose deprivation-induced tissue swelling, ROS production, and cell death in mouse brain with angiotensin II overproduction. *Neuroscience*. 2014;273:39–51.
- Somanna NK, Valente AJ, Krenz M, Fay WP, Delafontaine P, Chandrasekar B. The Nox1/4 dual inhibitor GKT137831 or Nox4 knockdown inhibits angiotensin-ii-induced adult mouse cardiac fibroblast proliferation and migration. AT1 physically associates with Nox4. *J Cell Physiol*. 2016;231(5):1130–41.
- Suzuki Y, Ruiz-Ortega M, Lorenzo O, Ruperez M, Esteban V, Egido J. Inflammation and angiotensin II. *Int J Biochem Cell Biol*. 2003;35(6):881–900.
- Liu G, Hosomi N, Hitomi H, Pelisch N, Fu H, Masugata H, Murao K, Ueno M, Matsumoto M, Nishiyama A. Angiotensin II induces human astrocyte senescence through reactive oxygen species production. *Hypertens Res*. 2011;34(4):479–83.
- Holappa M, Vapaatalo H, Vaajanen A. Local ocular renin-angiotensin-aldosterone system: any connection with intraocular pressure? A comprehensive review. *Ann Med*. 2020;52(5):191–206.

22. Wagner J, Jan Danser AH, Derkx FH, de Jong TV, Paul M, Mullins JJ, Schalekamp MA, Ganten D. Demonstration of renin mRNA, angiotensinogen mRNA, and angiotensin converting enzyme mRNA expression in the human eye: evidence for an intraocular renin-angiotensin system. *Br J Ophthalmol.* 1996;80(2):159–63.
23. Sramek SJ, Wallow IH, Tewksbury DA, Brandt CR, Poulsen GL. An ocular renin-angiotensin system. *Immunohistochemistry of Angiotensinogen. Invest Ophthalmol Vis Sci.* 1992;33(5):1627–32.
24. Murata M, Nakagawa M, Takahashi S. Angiotensinogen mRNA is synthesized locally in rat ocular tissues. *Ophthalmologica.* 1997;211(5):301–304.
25. Watkins RW, Baum T, Tedesco RP, Pula K, Barnett A. Systemic effects resulting from topical ocular administration of SCH 33861, a novel ACE inhibitor ocular hypotensive agent. *J Ocul Pharmacol.* 1988;4(2):93–100.
26. Abrams KL, Brooks DE, Laratta LJ, Barnhill MA, Frazier D. Angiotensin converting enzyme system in the normal canine eye: pharmacological and physiological aspects. *J Ocul Pharmacol.* 1991;7(1):41–51.
27. Keller KE, Bhattacharya SK, Borrás T, Brunner TM, Chansangpetch S, Clark AF, Dismuke WM, Du Y, Elliott MH, Ethier CR, Faralli JA, et al. Consensus recommendations for trabecular meshwork cell isolation, characterization and culture. *Exp Eye Res.* 2018;171:164–73.
28. Patel GC, Phan TN, Maddineni P, Kasetti RB, Millar JC, Clark AF, Zode GS. Dexamethasone-induced ocular hypertension in mice: effects of myocilin and route of administration. *Am J Pathol.* 2017;187(4):713–23.
29. Seki VBB, Souza GR, Messias A, Casarini DE, Paula JS. Aqueous humor renin, angiotensin I, and angiotensin II activity in primary open-angle glaucoma. *Arq Bras Oftalmol.* 2020;83(4):318–22.
30. Rosin NL, Falkenham A, Sopol MJ, Lee TD, Légaré JF. Regulation and role of connective tissue growth factor in AngII-induced myocardial fibrosis. *Am J Pathol.* 2013;182(3):714–26.
31. Jia Y, Xu J, Yu Y, Guo J, Liu P, Chen S, Jiang J. Nifedipine inhibits angiotensin II-induced cardiac fibrosis via downregulating Nox4-derived ROS generation and suppressing ERK1/2, JNK signaling pathways. *Pharmazie.* 2013;68(6):435–41.
32. Meng Y, Pan M, Zheng B, Chen Y, Li W, Yang Q, Zheng Z, Sun N, Zhang Y, Li X. Autophagy attenuates Angiotensin II-induced pulmonary fibrosis by inhibiting redox imbalance-mediated NOD-like receptor family pyrin domain containing 3 inflammasome activation. *Antioxid Redox Signal.* 2019;30(4):520–41.
33. Shen F, Zhang L, Liu T. [Effects of angiotensin II on the 3H-TdR incorporation and synthesis of collagen in cultured bovine trabecular meshwork cells]. *Yan Ke Xue Bao.* 2001;17(4):209–12.
34. Wang G, Anrather J, Huang J, Speth RC, Pickel VM, Iadecola C. NADPH oxidase contributes to angiotensin II signaling in the nucleus tractus solitarius. *J Neurosci.* 2004;24(24):5516–24.
35. Vermot A, Petit-Hartlein I, Smith SME, Fieschi F. NADPH oxidases (NOX): an overview from discovery, molecular mechanisms to physiology and pathology. *Antioxidants.* 2021;10(6):890.
36. Rao VR, Stubbs EB Jr. TGF-beta2 promotes oxidative stress in human trabecular meshwork cells by selectively enhancing NADPH oxidase 4 expression. *Invest Ophthalmol Vis Sci.* 2021;62(4):4.
37. Han ZN, Lin XX, Wang YY, Ding R, Hong L, Cui X. Cholecystokinin octapeptide promotes ANP secretion through activation of NOX4-PGC-1alpha-PPARalpha/PPARgamma signaling in isolated beating rat atria. *Oxid Med Cell Longev.* 2022;2022:5905374.
38. Giustarini D, Milzani A, Dalle -Donne I, Tsikas D, Rossi R. N-Acetylcysteine ethyl ester (NACET): a novel lipophilic cell-permeable cysteine derivative with an unusual pharmacokinetic feature and remarkable antioxidant potential. *Biochem Pharmacol.* 2012;84(11):1522–33.
39. Fuchshofer R, Tamm ER. The role of TGF-beta in the pathogenesis of primary open-angle glaucoma. *Cell Tissue Res.* 2012;347(1):279–90.
40. Dong Q, Li S, Wang W, Han L, Xia Z, Wu Y, Tang Y, Li J, Cheng X. FGF23 regulates atrial fibrosis in atrial fibrillation by mediating the STAT3 and SMAD3 pathways. *J Cell Physiol.* 2019;234(11):19502–10.
41. Liu XH, Zhang QY, Pan LL, Liu SY, Xu P, Luo XL, Zou SL, Xin H, Qu LF, Zhu YZ. NADPH oxidase 4 contributes to connective tissue growth factor expression through Smad3-dependent signaling pathway. *Free Radic Biol Med.* 2016;94:174–84.
42. Jinnin M, Ihn H, Tamaki K. Characterization of SIS3, a novel specific inhibitor of Smad3, and its effect on transforming growth factor-beta1-induced extracellular matrix expression. *Mol Pharmacol.* 2006;69(2):597–607.
43. Cao Y, Kumar S, Namkung Y, Gagnon L, Cho A, Laporte SA. Angiotensin II type 1 receptor variants alter endosomal receptor-beta-arrestin complex stability and MAPK activation. *J Biol Chem.* 2020;295(38):13169–80.
44. Azushima K, Morisawa N, Tamura K, Nishiyama A. Recent research advances in renin-angiotensin-aldosterone system receptors. *Curr Hypertens Rep.* 2020;22(3):22.
45. Shi H, Wang H, Fu S, Xu K, Zhang X, Xiao Y, Ye W. Losartan attenuates scar formation in filtering bleb after trabeculectomy. *Invest Ophthalmol Vis Sci.* 2017;58(3):1478–86.
46. Dikalov SI, Nazarewicz RR. Angiotensin II-induced production of mitochondrial reactive oxygen species: potential mechanisms and relevance for cardiovascular disease. *Antioxid Redox Signal.* 2013;19(10):1085–94.
47. Dikalov SI, Nazarewicz RR, Bikineyeva A, Hilenski L, Lassegue B, Griendling KK, Harrison DG, Dikalova AE. Nox2-induced production of mitochondrial superoxide in angiotensin II-mediated endothelial oxidative stress and hypertension. *Antioxid Redox Signal.* 2014;20(2):281–94.
48. Wang JN, Yang Q, Yang C, Cai YT, Xing T, Gao L, Wang F, Chen X, Liu XQ, He XY, Wei B, et al. Smad3 promotes AKI sensitivity in diabetic mice via interaction with p53 and induction of NOX4-dependent ROS production. *Redox Biol.* 2020;32:101479.
49. Lin YT, Chen JS, Wu MH, Hsieh IS, Liang CH, Hsu CL, Hong TM, Chen YL. Galectin-1 accelerates wound healing by regulating the neuropilin-1/Smad3/NOX4 pathway and ROS production in myofibroblasts. *J Invest Dermatol.* 2015;135(1):258–68.

50. Ozaki T, Nakazawa M, Yamashita T, Ishiguro S. Delivery of topically applied calpain inhibitory peptide to the posterior segment of the rat eye. *PLoS ONE*. 2015;10(6):e0130986.
51. Imanishi T, Hano T, Nishio I. Angiotensin II accelerates endothelial progenitor cell senescence through induction of oxidative stress. *J Hypertens*. 2005;23(1):97–104.
52. Herbert KE, Mistry Y, Hastings R, Poolman T, Niklason L, Williams B. Angiotensin II-mediated oxidative DNA damage accelerates cellular senescence in cultured human vascular smooth muscle cells via telomere-dependent and independent pathways. *Circ Res*. 2008;102(2):201–208.
53. Schafer MJ, White TA, Iijima K, Haak AJ, Ligresti G, Atkinson EJ, Oberg AL, Birch J, Salmonowicz H, Zhu Y, Mazula DL, et al. Cellular senescence mediates fibrotic pulmonary disease. *Nat Commun*. 2017;8:14532.
54. Liu RM, Liu G. Cell senescence and fibrotic lung diseases. *Exp Gerontol*. 2020;132:110836.